THE JOURNAL OF BIOLOGICAL CHEMISTRY
Vol. 278, No. 18, Issue of May 2, pp. 15941–15950, 2003

Printed in U.S.A.

Antithrombin III Phenylalanines 122 and 121 Contribute to Its High Affinity for Heparin and Its Conformational Activation*

Received for publication, December 4, 2002, and in revised form, January 28, 2003
Published, JBC Papers in Press, January 29, 2003, DOI 10.1074/jbc.M212319200

Mohamad Aman Jairajpuri‡, Aiqin Lu‡, Umesh Desai§, Steven T. Olson¶, Ingemar Bjork‖, and Susan C. Bock‡**

From the ‡Departments of Medicine and Bioengineering, University of Utah, Salt Lake City, Utah 84132, the §Department of Medicinal Chemistry, Virginia Commonwealth University, Richmond, Virginia 23298, the ¶Center for Molecular Biology of Oral Diseases, University of Illinois, Chicago, Illinois 60612, and the ‖Department of Veterinary Medical Chemistry, Swedish University of Agricultural Sciences, Uppsala SE-751 23, Sweden

The dissociation equilibrium constant for heparin binding to antithrombin III (ATIII) is a measure of the cofactor's binding to and activation of the proteinase inhibitor, and its salt dependence indicates that ionic and non-ionic interactions contribute ~40 and ~60% of the binding free energy, respectively. We now report that phenylalanines 121 and 122 (Phe-121 and Phe-122) together contribute 43% of the total binding free energy and 77% of the energy of non-ionic binding interactions. The large contribution of these hydrophobic residues to the binding energy is mediated not by direct interactions with heparin, but indirectly, through contacts between their phenyl rings and the non-polar stems of positively charged heparin binding residues, whose terminal amino and guanidinium groups are thereby organized to form extensive and specific ionic and non-ionic contacts with the pentasaccharide. Investigation of the kinetics of heparin binding demonstrated that Phe-122 is critical for promoting a normal rate of conformational change and stabilizing AT*H, the high affinity-activated binary complex. Kinetic and structural considerations suggest that Phe-122 and Lys-114 act cooperatively through non-ionic interactions to promote P-helix formation and ATIII binding to the pentasaccharide. In summary, although hydrophobic residues Phe-122 and Phe-121 make minimal contact with the pentasaccharide, they play a critical role in heparin binding and activation of antithrombin by coordinating the P-helix-mediated conformational change and organizing an extensive network of ionic and non-ionic interactions between positively charged heparin binding site residues and the cofactor.

The sulfated polysaccharide heparin functions as an anticoagulant by binding to antithrombin III (ATIII)[1] and greatly accelerating its rates of thrombin and factor Xa inhibition. Heparin binding to ATIII is a two-step process consisting of an initial weak interaction that induces a protein conformational change leading to the formation of a high affinity binary complex with the cofactor (AT*H) and ATIII activation (1, 2). Functional investigations of chemically modified, naturally occurring mutant and recombinant antithrombins have identified Arg-47, Lys-114, Lys-125, and Arg-129 as the most important positively charged amino acid residues in the heparin binding site of ATIII (3–12). Direct interactions of these basic residues with negatively charged groups of heparin are observed in the crystal structure of an ATIII-pentasaccharide complex (13). Studies of heparin binding kinetics indicate that Lys-125 is the most important amino acid in the initial docking with heparin and that Arg-129, Lys-114, and Arg-47 are critical for the protein conformational change step leading to the high affinity, activated AT*H complex. Heparin binding leads to elongation of ATIII helix D by 1.5 turns at its carboxyl-terminal end as well as the formation of a new alpha helix, the P-helix, at its amino-terminal end (13, 14). These structural changes are associated with expulsion of the P14 residue from central beta sheet A and increased reactivity with factor Xa (15, 16).

Protein-heparin interactions are comprised of ionic and non-ionic components whose energies and relative strengths can be measured using polyelectrolyte theory. For example, in the case of thrombin, 86% of the free energy of heparin binding results from ionic interactions, whereas 14% derives from non-ionic interactions (17). In contrast, for brain natriuretic peptide, non-ionic interactions contribute 94% of the heparin binding energy and only 6% is from ionic interactions (18). Antithrombin III heparin binding involves five to six ionic interactions that contribute only 40% of the binding energy (2, 17, 19). Non-ionic interactions are responsible for the remaining 60% of the binding energy. Although non-ionic interactions contribute more to the strength of ATIII heparin binding than do ionic interactions, work to date has focused mostly on arginines and lysines of the heparin binding site and ignored potentially important non-polar residues.

The present study was designed to address the roles of ATIII phenylalanines 121 and 122 (Phe-121 and Phe-122) in heparin binding and activation. Phe-121 and Phe-122 were selected for investigation based on their proximity to positively charged residues of the pentasaccharide binding site and because, although not conserved across different branches of the serpin family, these phenylalanines are conserved in antithrombins from different vertebrate species (20), which also conserve the capacity for heparin binding and activation (21).

The results of our work demonstrate that, although phenylalanines 121 and 122 make minimal direct contact with hep-

* This work was supported by American Heart Association Western States Affiliate Postdoctoral Fellowship 0020132Y (to M. A. J.), National Institutes of Health (NIH) Grant HL39888 (to S. T. O.), Swedish Medical Research Council Grant 4212 (to I. B.), and NIH Grant HL30712 (to S. C. B.). The costs of publication of this article were defrayed in part by the payment of page charges. This article must therefore be hereby marked "*advertisement*" in accordance with 18 U.S.C. Section 1734 solely to indicate this fact.

** To whom correspondence should be addressed: University of Utah Health Sciences Center, Pulmonary Division, 50 N. Medical Dr., Salt Lake City, UT 84132. Tel.: 801-585-6521; Fax: 801-585-3355; E-mail: susan.bock@m.cc.utah.edu.

[1] The abbreviations used are: ATIII, antithrombin III; HAH, full-length high affinity heparin; H5, heparin pentasaccharide; SI, stoichiometry of inhibition; *I*, ionic strength; PEG, polyethylene glycol.

arin, they nevertheless contribute significantly to antithrombin affinity for its cofactor and are responsible for 43% of the total binding energy and 77% of the free energy of non-ionic interactions. An F121A substitution decreased antithrombin affinity for heparin 13-fold, and an F122L substitution reduced heparin affinity >2000-fold through exclusively non-ionic effects. The large decrease in F122L affinity was due to a moderate decrease in the forward rate of the activating conformational change and greatly reduced stability of the AT*H complex. Binding equilibrium and kinetic data collected during the course of this work and information from the structure of an antithrombin-pentasaccharide complex also together suggest that Phe-122 and Lys-114 function cooperatively to coordinate the P-helix-mediated activating conformational change and to organize an extensive network of ionic and non-ionic interactions between positively charged antithrombin residues and heparin.

EXPERIMENTAL PROCEDURES

Materials—The Bac-to-Bac baculovirus expression system, Sf9 *Spodoptera frugiperda* cells, and Sf900II growth medium were obtained from Life Technologies, Inc. S2238 and S2765 were from Chromogenix. Human α-thrombin and pentasaccharide were the generous gifts of Drs. William Lawson and Maurice Petitou. Human factor Xa was purchased from Enzyme Research Laboratories. High affinity heparin (molecular mass, ~20,000 Da) was purified in our laboratory as previously described (22). High affinity heparin and pentasaccharide concentrations were determined by stoichiometric fluorescence titrations *versus* plasma antithrombin. Hi-Trap heparin and Sephacryl HR-300 columns were from Amersham Biosciences, and Econopak Q columns from Bio-Rad.

Buffers and Experimental Conditions—PNE buffer is 20 mM sodium phosphate, pH 7.4, 0.1 mM EDTA, 100 mM NaCl. QPNE buffer is PNE with a lower NaCl concentration (20 mM). PE buffer is PNE with no NaCl. Inhibition studies were conducted at 25 °C in PNE-PEG (PNE plus 0.1% PEG 6000). The ionic strength of pH 7.4 PNE-PEG is 0.15. Additional NaCl was added to PNE or PE to achieve different ionic strengths for binding studies as indicated.

Mutagenesis—F121A and F122L substitutions were made on a beta-ATIII background (N135A) to reduce heparin binding heterogeneity and facilitate purification (23). PCR-based megaprimer mutagenesis was as previously described (24) using the oligonucleotides 5′-CATCTGATCAAATCCACGCTTTCTTTGCCA-3′ for F121A and 5′-CATCTGATCAAATCCACTTCCTGTTTGCCAAAC-3′ for F122L and *Bst*YI digestion to identify mutant clones. Following sequence verification of the PCR-generated DNAs, *Nhe*I-*Sac*I fragments containing the substitutions were used to replace the corresponding portion of the human ATIII.N135A cDNA sequence cloned in pFastbac1, followed by transposition and virus production in the Bac-to-Bac expression system.

ATIII Purification—Supernatants from baculovirus-infected Sf9 cultures were harvested and cleared of cells and debris at 4–5 days post infection, when the trypan blue viability of the host cells had dropped to ~80%. 20-ml Hi-Trap heparin affinity columns were loaded with 0.22-μm filtered supernatants diluted 1:1 with PE, washed with PE, and eluted with a 100 ml of 0.02–2.4 M NaCl gradient. Fractions containing the peak of inhibitory activity against thrombin were pooled, concentrated, and buffer-exchanged in tangential flow centrifugal concentrators. The sample in ~1 ml was applied to a 2.6- × 60-cm Sephacryl S-300 column. Fractions containing the peak of thrombin inhibitory activity were pooled, concentrated, and buffer-exchanged into PE. The sample was subjected to another round of heparin affinity chromatography as described above, but using a 5-ml column. The fractions with peak thrombin inhibitory activity were pooled, concentrated, and buffer-exchanged into QPNE. The sample was applied to a 5-ml Econopak Q column in QPNE and eluted with a 45-ml 0.02–0.6 M NaCl gradient. The peak of thrombin inhibitory activity was concentrated and buffer-exchanged into PNE. SDS-PAGE was also used to monitor purification steps and to assess the purities of the recombinant antithrombins. Protein concentrations of the purified F121A/N135A and F122L/N135A were determined from absorbance at 280 nm using the molar extinction coefficient of plasma ATIII (25).

Stoichiometries, Affinities, and Ionic Strength Dependence of Heparin Binding—Stoichiometries and dissociation equilibrium constants (K_d) for pentasaccharide and full-length heparin binding to ATIII variants were determined by titrations monitored by the tryptophan fluorescence enhancement that accompanies the binding interaction as previously described (22, 26). Stoichiometric titrations were performed with full-length heparin at an ionic strength of 0.10, using antithrombin concentrations based on absorbance measurements that were more than 10 times the K_d. Pentasaccharide and full-length heparin binding to antithrombin for K_d titrations used active ATIII concentrations obtained from the heparin binding stoichiometries. Ionic and non-ionic components of heparin binding to the F121A/N135A, F122L/N135A, and N135A antithrombins were obtained from the ionic strength dependence of the dissociation equilibrium constant for full-length heparin at pH 7.4 and for heparin pentasaccharide at pH 6.0. Derivation of Z, the number of ionic interactions involved in the binding, and K_d', which indicates the strength of non-ionic interactions, is discussed in detail under "Results."

Kinetics of Heparin Binding—Heparin binds to antithrombin according to the two-step, induced-fit mechanism depicted in Scheme I (19, 27, 28) as follows.

$$\mathrm{AT} + \mathrm{H} \underset{}{\overset{K_1}{\longleftrightarrow}} \mathrm{AT\text{-}H} \underset{k_{-2}}{\overset{k_{+2}}{\longleftrightarrow}} \mathrm{AT^*H}$$

SCHEME 1

In this scheme, K_1 is the dissociation equilibrium constant for the initial binding of antithrombin III (AT) and heparin (H), which leads to the formation of a low affinity complex, AT-H. k_{+2} is the forward rate constant for the subsequent rapid conformational change leading to the high affinity activated complex, AT*H, and k_{-2} is the reverse rate constant for this step, and is equivalent to k_{off} for the overall reaction. The two-step binding mechanism leads to a hyperbolic dependence of k_{obs}, the pseudo-first-order rate constant, on total heparin concentration ($[H]_o$), as described by Equation 1,

$$k_{obs} = ((k_{+2}[H]_o)/([H]_o + K_1)) + k_{-2} \quad \text{(Eq. 1)}$$

k_{on} and k_{off} ($= k_{-2}$) for the overall reaction can be obtained from the initial slope and y-intercept of a linear regression of a k_{obs} *versus* [heparin] plot at low heparin concentrations, whereas K_1 and k_{+2} can be determined by non-linear regression of hyperbolic plots of k_{obs} *versus* $[H]_o$ extending to higher heparin concentrations that approach saturation.

The kinetics of full-length heparin and pentasaccharide binding to F122L/N135A were analyzed at 25 °C under two conditions of pH and ionic strength (pH 7.4, 0.15 I and pH 6.0, 0.075 I). Binding was performed under pseudo-first-order conditions by maintaining a heparin to antithrombin molar ratio of ≥5:1, and the binding reactions were followed kinetically by monitoring the protein fluorescence increase with a stopped-flow fluorometer (Applied Photophysics SX-17MV). Progress curves from 5 to 12 binding reactions were fit to a single-exponential function to obtain the average k_{obs} at different cofactor concentrations, ranging from 0.2 to 25 μM for full-length heparin, and from 0.2 to 100 μM for pentasaccharide. k_{on} and k_{off} (k_{-2}) for the overall bimolecular reaction and K_1 and k_{+2} of Scheme 1 were determined by linear and non-linear regression fitting, respectively, of the initial linear and overall hyperbolic plots of k_{obs} *versus* $[H]_o$ to Equation 1 using GraphPad Prism and Kaleidagraph software. Calculated K_d values for heparin binding to F122L/N135A were obtained by dividing the measured k_{off} value by the measured k_{on} value.

Thrombin and Factor Xa Inhibition—Inhibition stoichiometries (SI) for thrombin and factor Xa and apparent second order rate constants (k_{app}) for the inhibition of these enzymes by F121A/N135A, F122L/N135A and their N135A parent were measured in the absence and presence of pentasaccharide and full-length heparin as previously described (22). Association rate constants (k_{assoc}) were obtained by correcting k_{app} values for the content of inactive material in the sample and/or substrate pathway partitioning by multiplying the average of 2–3 k_{app} measurements by the SI value obtained for the same ATIII-target enzyme-heparin combination.

Structural Analysis—The I chains from a 2.62-Å resolution structure of human plasma α-antithrombin (Protein Data Bank, pdb.1E05) and a 2.90-Å resolution structure of human plasma α-ATIII bound to pentasaccharide (pdb.1E03) were viewed and analyzed using QUANTA software.

RESULTS

Expression and Purification—F121A/N135A and F122L/N135A recombinant antithrombins and their N135A parent

were expressed in the baculovirus system. The parental N135A molecule corresponds to the naturally occurring β isoform of antithrombin III, which is not glycosylated on asparagine-135. The N135A β isoform background facilitates investigation of antithrombin-heparin interactions by eliminating the heparin binding heterogeneity resulting from partial modification of Asn-135 and the associated production of α and β glycoforms when the wild type *N*-glycosylation consensus sequence (asparagine-proline-serine) is present at residues 135–137 (23, 29). The higher heparin affinity of the β antithrombin isoform, relative to the α antithrombin isoform, is experimentally advantageous with respect to purification and increased heparin binding affinity of the control. The pentasaccharide binding site of ATIII β (pdb.1E04) resembles that of ATIII α (pdb.1E05), and previous studies have shown that conclusions about the mechanism of heparin binding and activation obtained from investigation of β antithrombin mutants (N135A background) apply to the antithrombin α isoform as well (31). The purification of F121A/N135A and F122L/N135A from supernatants of baculovirus-infected Sf9 cells involved heparin affinity, gel exclusion, and anion exchange chromatography steps. Purified F121A/N135A, F122L/N135A, and N135A comigrated on SDS-PAGE and were >95% homogeneous.

Affinities of F121A/N135A and F122L/N135A Binding to Full-length Heparin and Pentasaccharide—Heparin affinity column elution behavior during chromatographic purification of the antithrombins suggested that the F121A substitution moderately reduced affinity for heparin and that the F122L substitution greatly decreased heparin binding. In contrast to control N135A antithrombin, which eluted from immobilized heparin at ~2.2 M NaCl, F121A/N135A eluted at 1–1.3 M NaCl, and F122L/N135A at 0.2–0.3 M NaCl.

Binding stoichiometries and affinities of the mutant and control antithrombins for heparin and pentasaccharide were measured by titrations monitored by the fluorescence enhancement resulting from protein conformation-dependent changes in tryptophan environment (1, 30). Compared with the 40% increase reported for the N135A control and plasma-derived antithrombin (23), full-length heparin induced an intrinsic fluorescence enhancement of ~10% for F121A/N135A, and ~30% for F122L/N135A. Heparin binding stoichiometries were 0.8 for two preparations of F121A/N135A, 0.8 and 1.0 for two preparations of F122L/N135A, and 0.6–0.8 for several preparations of N135A.

Table I presents dissociation equilibrium constant data for N135A, F121A/N135A, and F122L/N135A binding to full-length high affinity heparin and pentasaccharide under ionic strength conditions where the binding could be experimentally measured. Full-length heparin titrations were conducted at pH 7.4, and pentasaccharide titrations at pH 6.0. The K_d obtained for high affinity heparin binding to the N135A control at pH 7.4 and 0.3 *I* was similar to previously reported values (23, 31). K_d values for heparin binding to the two mutant inhibitors revealed that, although both bound heparin less tightly, the magnitude of their affinity losses differed significantly. Measurements at 0.3 and 0.4 *I* demonstrated an overall affinity loss of ~13-fold for F121A/N135A compared with its N135A parent. Based on measurements made at 0.3 and 0.15 *I*, the F122L substitution induced a more substantial ~2000-fold decrease in affinity for full-length heparin. Comparison of K_d values for F122L/N135A binding to pentasaccharide at pH 6.0 and 0.025 and 0.075 *I* with previously published K_d values for the N135A control extrapolated to these ionic strengths (11) revealed a 3000- to 4000-fold loss in F122L/N135A affinity for the core sequence of anticoagulant heparin.

TABLE I

Dissociation equilibrium constants for full-length heparin and pentasaccharide binding to F121A/N135A, F122L/N135A, and N135A antithrombin variants at 25 °C

Dissociation equilibrium constants (K_d) for full-length heparin (HAH) binding were determined from fluorescence titrations at pH 7.4 and the indicated ionic strengths. K_d for pentasaccharide (H5) binding to F122L/N135A were measured at pH 6.0 and the indicated ionic strengths.

Heparin form	pH	ATIII variant	Ionic strength	K_d
				*n*M
HAH	7.4	N135A	0.40	17 ± 2[a]
		F121A/N135A	0.40	210 ± 70[b]
		N135A	0.30	3 ± 1[b]
		F121A/N135A	0.30	38 ± 8[a]
		F122L/N135A	0.30	6700 ± 510[a]
		N135A	0.15	−0.2[c,d]
		N135A	0.15	−0.1[e]
		F122L/N135A	0.15	280 ± 25[a]
H5	6.0	N135A	0.075	0.020[d,f]
		F122L/N135A	0.075	68 ± 5[b]
		N135A	0.025	0.0002[d,f]
		F122L/N135A	0.025	0.8 ± 0.1[a]

[a] Average ± S.E. of three titrations.
[b] Average ± range of two titrations.
[c] Data from Ref. 23.
[d] Estimated by linear extrapolation of data from titrations at higher ionic strengths.
[e] Estimated by linear extrapolation of data from titrations in Fig. 1.
[f] Data from Ref. 11.

Ionic and Non-ionic Components of F121A/N135A and F122L/N135A Binding to Full-length Heparin and Pentasaccharide—The strengths of the ionic and non-ionic components of the overall binding interaction between antithrombin and heparin can be quantified by *Z*, the number of ionic interactions involved in the binding, and K_d', the dissociation constant in 1 M Na^+, which reflects the strength of non-ionic interactions (2, 17). Hydrogen bonds, although electrostatic in nature, are classified as non-ionic interactions in this analysis, because the ionic interactions measured by the technique include only ion pair-type interactions. For a given antithrombin-heparin combination, values of *Z* and K_d' were determined from Equation 2, which describes the sodium ion dependence of the observed overall dissociation constant $K_{d,obs}$, with *Z* and K_d' defined as above, and Ψ being the fraction of Na^+ bound per heparin charge and released upon binding to antithrombin (estimated to be 0.8 (17)).

$$\log K_{d,obs} = \log K_d' + Z\psi \log[Na^+] \quad \text{(Eq. 2)}$$

Fig. 1 shows that, in accordance with Equation 2, the logarithms of Table I K_d values (and additional K_d values obtained from titrations at other ionic strengths) varied linearly with the logarithms of the sodium concentrations at which they were measured. *Z* and log K_d' values presented in Table II were derived from the slopes and intercepts of linear regression fits for each antithrombin-heparin pair in Fig. 1. At pH 7.4, approximately six ionic interactions participate in the binding of the full-length heparin to the N135A control, whereas at pH 6, approximately five ionic interactions participate in binding of the pentasaccharide, in agreement with measurements from previous work (2, 19). *Z* values for F121A/N135A and F122L/N135A binding to full-length heparin and pentasaccharide were not significantly different from corresponding *Z* values for the N135A parent, indicating that the observed 13-fold and >2000-fold binding affinity losses are occurring without changing the number of ionic interactions between the mutants and the heparins. Table II also shows 30-, 1600-, and 5000-fold losses in the strengths of non-ionic interactions for the binding

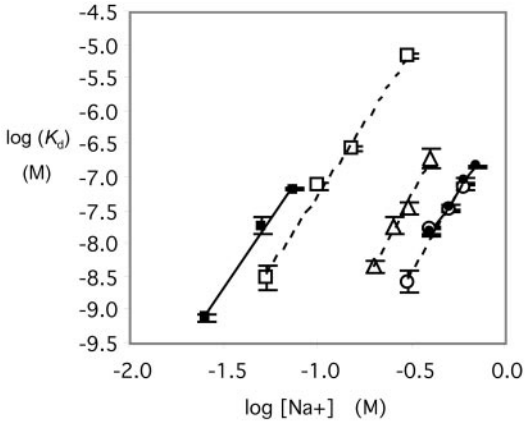

FIG. 1. **Ionic strength dependence of the dissociation equilibrium constant for full-length heparin binding to N135A, F121A/N135A, and F122L/N135A at pH 7.4, 25 °C and for pentasaccharide binding to N135A and F122L/N135A at pH 6.0, 25 °C.** Each *point* represents the average ± S.E. for 2–5 titrations at the indicated ionic strength. Not visible are *error bars* that lie within the dimensions of the symbols. *Lines* show the linear regression fits used to determine Z and K_d' values (Table II) for antithrombin interactions with full-length heparin at pH 7.4 (*dotted lines*) and pentasaccharide at pH 6.0 (*solid lines*). The data for the interaction of pentasaccharide with the N135A control were taken from previously published work (11) and are provided for comparison. *Open circles*, HAH-N135A; *open triangles*, HAH-F121A/N135A; *open squares*, HAH-F122L/N135A; *solid circles*, H5-N135A; *solid squares*, H5-F122L/N135A.

TABLE II
Ionic and non-ionic components of heparin binding to the F121A/N135A, F122L/N135A, and N135A antithrombin variants at 25 °C

The number of ionic interactions (Z) involved in the binding of pentasaccharide (H5) or full-length heparin (HAH) to the antithrombin variants, and the non-ionic contribution ($\log(K_d')$) to the overall binding interaction were determined from the slopes and intercepts, respectively, of the Fig. 1 $\log(K_d)$ *versus* $\log[Na^+]$ plots. Errors represent ± S.E. obtained by linear regression.

Heparin form	pH	ATIII variant	Z	$\text{Log}(K_d')$
HAH	7.4	N135A	5.9 ± 0.6	−6.1 ± 0.2
		F121A/N135A	6.6 ± 0.4	−4.6 ± 0.2
		F122L/N135A	5.5 ± 0.3	−2.9 ± 0.2
H5	6.0	N135A	5.2 ± 0.2[a]	−6.2 ± 0.1[a]
		F122L/N135A	5.1 ± 0.5	−2.5 ± 0.5

[a] Data from Ref. 11.

of F121A/N135A to full-length heparin, F122L/N135A to full-length heparin, and F122L/N135A to pentasaccharide, based on increases of 1.5, 3.2, and 3.7 in the $\log(K_d')$, respectively. Both the moderate loss of heparin binding affinity due to substitution of phenylalanine 121 with alanine and the large loss of heparin binding affinity due to substitution of phenylalanine 122 with leucine were entirely accounted for by reductions in the non-ionic components of the binding interactions.

The contributions of phenylalanines 121 and 122 to the free energy of full-length heparin binding to ATIII were calculated from Table I and Fig. 1 pH 7.4 dissociation equilibrium constant data. The K_d for F122L/N135A was measured at 0.15 I, whereas those for N135A and F121A/N135A were extrapolated from measurements made at higher ionic strengths. Using $\Delta G^0 = -RT \ln(K_d)$, total binding energies were calculated and yielded values of 59.0, 53.4, and 39.0 kJ/mole for N135A, F121A/N135A, and F122L/N135A, respectively. The magnitudes of the ATIII variant binding energy losses indicate that Phe-121 and Phe-122 together contribute 43% of the total free energy of full-length heparin binding to ATIII at physiological pH and ionic strength. A similar analysis using $\log K_d'$ values obtained at pH 7.4 (Table II) yielded values of 36.3, 27.4, and 17.3 kJ/mole, respectively, for the non-ionic binding energies of N135A, F121A/N135A, and F122L/N135A with full-length heparin. The associated binding energy losses indicate that Phe-121 and Phe-122 together contribute 77% of the non-ionic binding energy.

Kinetic Analysis of Full-length Heparin and Pentasaccharide Binding to F122L/N135A—Rapid kinetic analysis of full-length heparin and pentasaccharide binding to F122L/N135A was performed to determine which step or steps of the two-step induced fit binding mechanism (Scheme I) are affected by the F122L mutation and responsible for the >2000-fold reduction in binding affinity. For the binding of F122L/N135A to 0.2–25 μM HAH at pH 7.4, 0.15 I and for its binding to 0.2–12 μM H5 at pH 6.0, 0.075 I, k_{obs} exhibited a hyperbolic dependence on heparin concentration as illustrated in *panels A* and *B* of Fig. 2. However, k_{obs} for F122L/N135A binding to pentasaccharide at pH 7.4 and 0.15 I was linear through at least 100 μM H5 (Fig. 2*C*). Table III presents kinetic constants for the binding reactions derived by fitting the data of Fig. 2 to Equation 1 as described under "Experimental Procedures" and in the figure legend. Calculated K_d values were obtained by dividing k_{off} by k_{on} and were in general agreement with measured K_d values for binding to full-length heparin at pH 7.4 and 0.15 I, and binding to pentasaccharide at pH 6.0 and 0.075 I. The similarity of the K_d values determined by different methods supports the validity of data obtained by stopped-flow and fluorescence titration experiments. The somewhat larger difference between the calculated and measured K_d values for pentasaccharide binding at pH 6.0, 0.075 I may reflect a small contribution of the pre-equilibrium pathway in this case (9).

Analysis of Table III data shows that the overall effect of the F122L substitution is to both reduce the k_{on} values and increase the k_{off} values for heparin and pentasaccharide binding. However, the extent to which k_{on} and k_{off} are altered varies with the type of heparin and the binding conditions. For the interaction of F122L/N135A with full-length heparin at pH 7.4 and 0.15 I, the overall association rate constant k_{on} was reduced ~15-fold, and the overall dissociation rate constant k_{off} was increased by ~235-fold. The reduction in k_{on} could be entirely accounted for by a similar reduction in k_{+2}, the forward rate constant for the conformational change step leading to the activated AT*H complex, and there was no evidence for an increase in K_1, the dissociation equilibrium constant for the initial binding step leading to the AT-H intermediate. Under the same conditions (pH 7.4 and 0.15 I), F122L/N135A binding to pentasaccharide exhibited an ~120-fold decrease in k_{on} and a ~120-fold increase in k_{off}. Although the magnitude of the k_{off} increase was similar to that observed with full-length heparin, the magnitude of the k_{on} decrease was almost one log higher than with HAH. Moreover, the linearity of the dependence of k_{obs} on [H5] in the concentration range studied (Fig. 2*C*) indicates that the more severe k_{on} defect for pentasaccharide binding is due to an increase in K_1 that is not observed with full-length heparin.

K_1 and k_{+2} contributions to k_{on} for the binding of F122L/N135A and pentasaccharide were measured under pH 6.0 and 0.075 I conditions, where binding is tighter and k_{obs} displayed a hyperbolic dependence on [H5] at reasonable concentrations of pentasaccharide (Fig. 2*B*). Under these conditions, the loss of binding affinity is overwhelmingly due to a very large ~1600-fold increase in k_{off}. However, there is also a modest 7-fold decrease in k_{on}, and it was possible to discern from the non-linear regression fit that this k_{on} reduction derived from a 3-fold increase in K_1 (the dissociation equilibrium constant for the weak AT-H intermediate) and a 3-fold decrease in k_{+2} (the

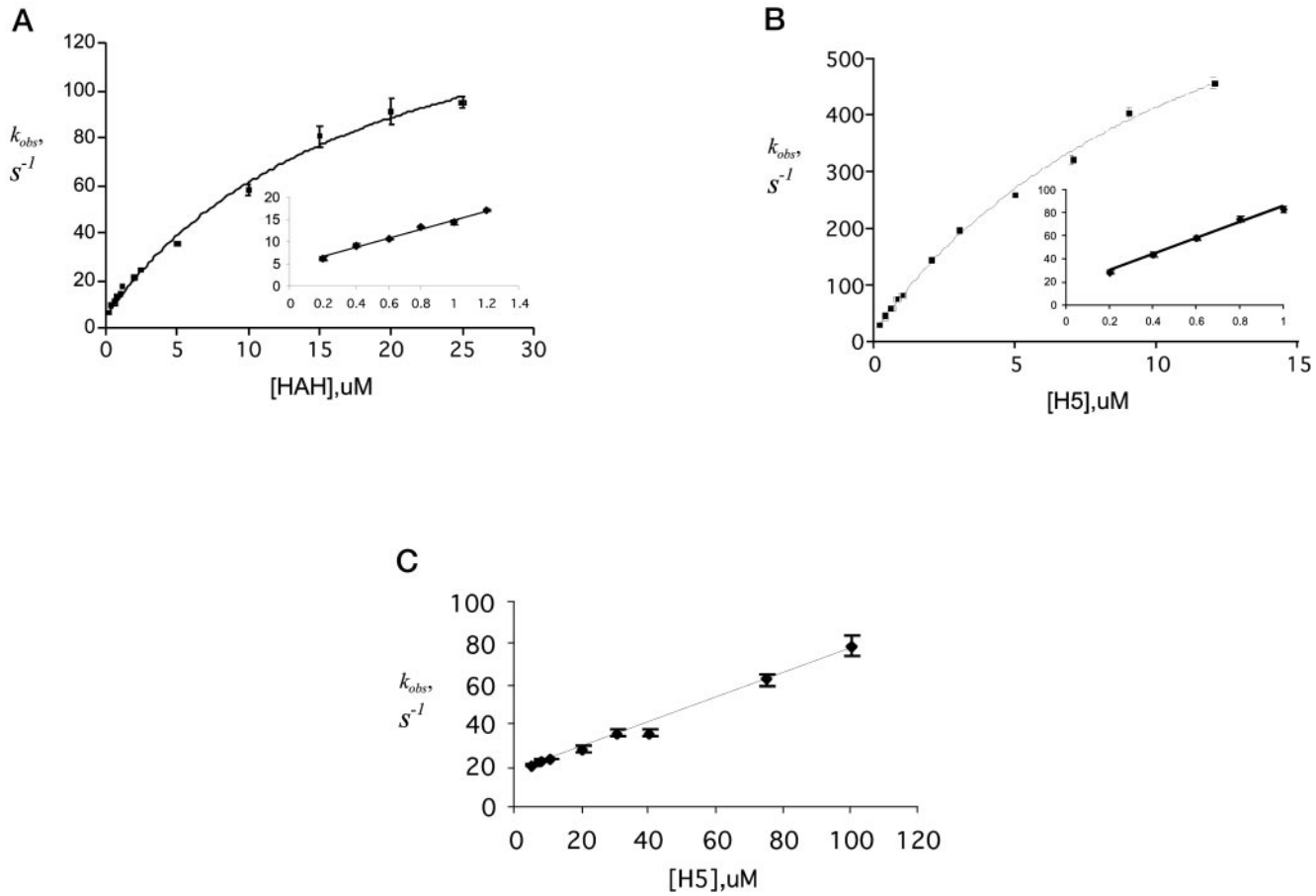

FIG. 2. **Kinetics of full-length heparin and pentasaccharide binding to F122L/N135A.** Plots show the linear and hyperbolic dependence of k_{obs} on heparin concentration under various conditions. *A*, full-length heparin (*HAH*) binding to F122L/N135A at pH 7.4, 0.15 *I*, 25 °C. *B*, pentasaccharide (*H5*) binding to F122L/N135A at pH 6.0, 0.075 *I*, 25 °C. *C*, pentasaccharide (*H5*) binding to F122L/N135A at pH 7.4, 0.15 *I*, 25 °C. Average values ± S.E. for 5–12 measurements at each HAH or pentasaccharide concentration are plotted. Not visible are *error bars* that lie within the dimensions of the symbols. The k_{on} and k_{off} values in Table III were obtained by linear regression fitting of data points in *A* and *B insets* and *panel C* to Equation 1. The K_1 and k_{+2} values in Table III were obtained by non-linear regression fitting of data from the full range of heparin concentrations in *A* and *B* to Equation 1 using k_{off} values determined at low concentrations for k_{-2}.

TABLE III

Measured kinetic constants, bimolecular association rate constants, dissociation rate constants, and calculated dissociation equilibrium constants for full-length heparin and pentasaccharide binding to F122L/N135A at 25 °C

K_1 and k_{+2} were obtained by non-linear regression fitting of the hyperbolic curves in Fig. 2 to Equation 1. k_{on} and k_{off} were obtained by regression using 5–8 points from the initial linear regions of the Fig. 2 k_{obs} *versus* [HAH] or [H5] plots. Errors are ± S.E. of the fits. Calculated K_d values were obtained by dividing k_{off} by k_{on}. N135A control data are from previously published studies as indicated in the footnotes and are provided for facile comparison.

ATIII variant	pH	*I*	Heparin form	K_1	k_{+2}	10^{-6} k_{on}	k_{off}	K_d	
								Calculated	Measured
				μM	s^{-1}	M^{-1} s^{-1}	s^{-1}	*nM*	*nM*
N135A	7.4	0.15	HAH	≥10[a]	≥3000[a]	154 ± 1[b]	≈0.02[b,c]		≈0.15[b,d]
F122L/N135A				19 ± 2	160 ± 11	10.0 ± 0.5	4.7 ± 0.4	≈470	280 ± 25[e]
N135A	7.4	0.15	H5	28 ± 4[b]	2100 ± 300[b]	70 ± 2[b]	0.14 ± 0.07[b,c]		2 ± 1[b,d]
F122L/N135A				ND[f]	ND	0.6 ± 0.03	17 ± 1.2	≈28,000	ND
N135A	6.0	0.075	H5	4 ± 0.7[g]	2100 ± 300[g]	520 ± 5[c,d,h]	0.01[h]	0.02	0.02[d,h]
F122L/N135A				11 ± 1	800 ± 30	70 ± 4	16.5 ± 2.6	≈228	68 ± 5[e]

[a] Data from Ref. 19.
[b] Data from Ref. 9.
[c] Calculated from K_d and k_{on}.
[d] Estimated by linear extrapolation of data from titrations at higher ionic strengths.
[e] Provided from Table I, for facile comparison.
[f] ND, Not determined.
[g] Based on estimates reported in Ref. 11.
[h] Data from Ref. 11.

forward rate constant for the conformational change leading to AT*H). The identification of a K_1 defect for F122L/N135A binding to pentasaccharide, considered in conjunction with the normal K_1 for F122L/N135A binding to full-length heparin, suggests that the extra oligosaccharide residues of full-length heparin compensate for the decreased ability of the pentasac-

TABLE IV
Association rate constants of N135A, F121A/N135A, and F122L/N135A with thrombin and factor Xa in the absence and presence of full-length heparin or pentasaccharide at pH 7.4, 0.15I, and 25 °C

Apparent rate constants (k_{app}) and stoichiometries (SI) for the inhibition of thrombin and factor Xa in the absence (*uncat*) of cofactor and the presence full-length heparin (*HAH*) or pentasaccharide (*H5*) were measured at pH 7.4, 0.15*I,* and 25°C as described under "Experimental Procedures." Association rate constants (k_{assoc}) were obtained by multiplying the k_{app} and SI values to correct for the content of inactive material in the preparation and for substrate partitioning. Tabulated values are average ± S.E. for 3–9 measurements, except as noted.

Target enzyme	Heparin form	Antithrombin variant	k_{assoc}
			$M^{-1}\ s^{-1}$
Thrombin	uncat	N135A	$6.9 \pm 0.2 \times 10^{3}$[a]
		F121A/N135A	$6.8 \pm 0.5 \times 10^{3}$
		F122L/N135A	$2.7 \pm 0.3 \times 10^{3}$
	HAH	N135A	$6.1 \pm 0.6 \times 10^{6}$[a]
		F121A/N135A	$1.1 \pm 0.2 \times 10^{7}$
		F122L/N135A	$3.2 \pm 0.0 \times 10^{7}$
	H5	N135A	$1.2 \pm 0.1 \times 10^{1}$[a]
		F121A/N135A	$7.1 \pm 0.3 \times 10^{3}$[b]
		F122L/N135A	$3.4 \pm 0.4 \times 10^{3}$[b]
Factor Xa	uncat	N135A	$4.3 \pm 0.4 \times 10^{3}$[a]
		F121A/N135A	$2.0 \pm 0.2 \times 10^{3}$
		F122L/N135A	$2.1 \pm 0.1 \times 10^{3}$
	HAH	N135A	$9.2 \pm 0.2 \times 10^{5}$[a]
		F121A/N135A	$2.2 \pm 0.0 \times 10^{6}$
		F122L/N135A	$4.0 \pm 0.0 \times 10^{6}$
	H5	N135A	$5.0 \pm 0.2 \times 10^{5}$[a]
		F121A/N135A	$4.6 \pm 0.5 \times 10^{5}$
		F122L/N135A	$5.2 \pm 1.5 \times 10^{6}$[c]

[a] From Ref. 19.
[b] Rates of F121A/N135A- and F122L/N135A-mediated thrombin inhibition did not increase above uncatalyzed rates following the addition of pentasaccharide and prolonged incubation of these reactions. Therefore, H5-dependent k_a rates were calculated by multiplying the k_{app} for the uncatalyzed reaction by SIs determined in the presence of pentasaccharide.
[c] This value is subject to uncertainty associated with utilization of the large calculated K_d for low afffinity F122L/N135A binding to pentasaccharide (28 mM, Table III) in the k_a to k_{assoc} conversion.

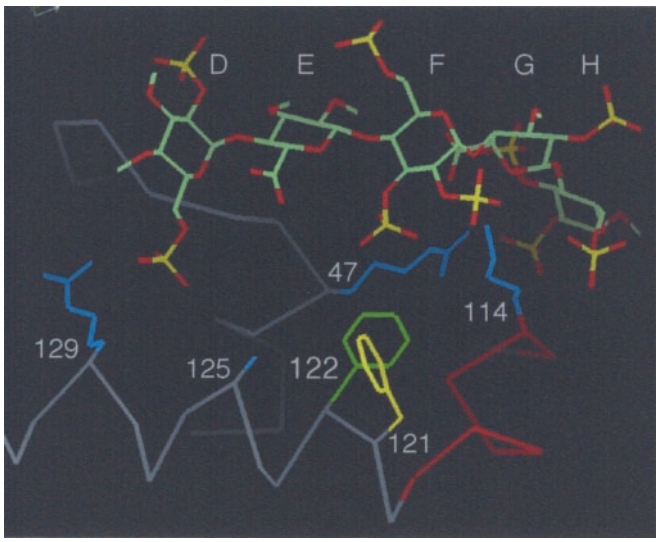

FIG. 3. **Phe-121 and Phe-122 are located in the center of a cluster of positively charged heparin binding residues under the bound pentasaccharide.** The pentasaccharide-binding region from the *I*-chain of pdb.1E03 is shown. Phe-121 side chain is *yellow*. Phe-122 side chain is *green*. Arg-47, Lys-114, Lys-125, and Arg-129 side chains are *blue*. The α carbon trace of antithrombin III is *gray*, except for residues 113–119, which form the P-helix and are drawn in *red*. All non-hydrogen atoms of the pentasaccharide are shown, with carbon in *green*, oxygen in *red*, and sulfur in *yellow*. Individual sugars of the pentasaccharide are denoted in *alphabetical order* from the nonreducing end.

TABLE V
Packing of Phe-122 against Arg-47 and Lys-114

Van der Waals and hydrophobic contacts of Phe-122 atoms with Arg-47 and Lys-114 atoms in the *I*-chain of antithrombin-pentasaccharide complex (pdb.1E03).

Interaction	Distance
	Å
F122_CD1 - R47_CB	4.3
F122_CE1 - R47_CG	4.6
F122_CZ - R47_CD	3.5
F122_CE2 - K114_CD	4.3
F122_CZ - K114_CE	4.7

charide to form the low affinity AT-H intermediate with the F122L/N135A mutant. This might be accomplished by the larger heparin providing an electrostatic guiding effect that enhances the initial rate of association.

Thrombin and Factor Xa Inhibition—Table IV lists the association rates (k_{assoc}) of F121A/N135A and F122L/N135A with thrombin and factor Xa in the absence and presence of full-length heparin or pentasaccharide. Association rates were obtained by measuring the apparent inhibition rate (k_{app}) and stoichiometry of inhibition (SI) for the different ATIII-target enzyme-cofactor combinations at pH 7.4 and 0.15 *I* and corrected for the content of inactive material and/or substrate partitioning by multiplying $k_{app} \times$ SI. Values of k_{assoc} for F121A/N135A and F122L/N135A inhibition of thrombin and factor Xa in the absence and presence of full-length heparin and pentasaccharide are similar to previously published values for the control N135A molecule (19). Therefore, F121A/N135A and F122L/N135A are properly folded and exhibit the same profiles of full-length heparin and pentasaccharide activation of proteinase inhibition observed for plasma antithrombin and the control recombinant ATIII. Specifically, the reactivities (k_{assoc}) of F121A/N135A and F122L/N135A with thrombin and factor Xa were accelerated three orders of magnitude by full-length heparin, whereas pentasaccharide-mediated factor Xa inhibition rates increased by only two orders of magnitude, and thrombin inhibition was minimally stimulated by the addition of pentasaccharide.

Although the initial rates for association of F121A/N135A and F122L/N135A and their heparin complexes with thrombin and factor Xa are normal, stoichiometry of proteinase inhibition data indicate that, following acylation with the target enzyme, partitioning into the substrate arm of the branched pathway of serpin inhibition is increased compared with the N135A control. Stoichiometries for F121A/N135A uncatalyzed inhibition of thrombin and factor Xa were in the 3.3–4.4 range. In the presence of pentasaccharide, inhibition stoichiometries ranged from 3.6 to 4.2, and in the presence of full-length heparin, values between 4.8 and 5.4 were obtained. In contrast, the heparin binding stoichiometry for F121A/N135A was 0.8, which would correspond to a proteinase inhibition SI of 1.25 if all heparin-binding molecules in the sample were competent for proteinase inhibition *and* no substrate partitioning occurred. The mismatch between the proteinase inhibition stoichiometries and the heparin binding stoichiometry of F121A/N135A suggests that Phe-121 plays a role in promoting ATIII

TABLE VI

Ionic and non-ionic contacts of antithrombin residues Arg-47 and Lys-114 with bound pentasaccharide

Distances between the indicated atoms of antithrombin residues Arg-47 or Lys-114 and bound pentasaccharide were measured in the *I*-chain of pdb.1E03.

Interaction type	Lys-114	Pentasaccharide[a]	Distance	Interaction type	Arg-47	Pentasaccharide[a]	Distance
			Å				Å
Hydrophobic vdW	CB	Sugar H C5F	4.3	H bond	NH2	Sugar H O5A	3.1
Hydrophobic	CG	Sugar H C50	4.6	H bond	NH2	Sugar H O51	2.7
H bond	NZ	F/G *O*-linkage	3.2	Ionic	NH2	Sugar H O5O	3.5
H bond	NZ	Sugar G 042	2.7	Ionic	NH1	sugar H O51	3.5
H bond	NZ	Sugar G O45	2.8	Ionic	NE	sugar G O45	3.4
Ionic	NZ	Sugar F O3C	3.4	Ionic	NE	sugar F O3F	4.1
Ionic	NZ	Sugar F O31	3.5				
Ionic	NZ	Sugar H O56	3.7				

[a] Atoms of pentasaccharide are identified by sugar ring and identification code from the 1E03 pdb file.

utilization of the complex formation arm, rather than the substrate pathway arm, of the branched serpin inhibition pathway. Consistent with this alternative, a band with the mobility of cleaved antithrombin was readily observed on non-reducing SDS-polyacrylamide gels of F121A/N135A complex formation reactions (data not shown). Stoichiometries for F122L/N135A inhibition of thrombin and factor Xa in the absence of heparin were in the 1.9–2.0 range. In the presence of pentasaccharide they ranged from 2.4 to 2.5, whereas in the presence of full-length heparin, values between 2.3 and 2.6 were obtained. The heparin binding stoichiometry for F122L/N135A ranged from 0.8 to 1.0. Small amounts of a band with the mobility of cleaved antithrombin were also observed on non-reducing SDS-polyacrylamide gels of F122L/N135A complex formation reactions (data not shown). The gel data and the mismatch between the proteinase inhibition stoichiometries and the heparin binding stoichiometry of F122L/N135A suggest that the wild type Phe-122 residue of antithrombin III also contributes to blocking flux through the substrate arm of the branched pathway, however, its importance in this regard is less than that of the adjacent Phe-121 residue. The observed substrate tendencies of the F121A/N135A and F122L/N135A variants imply that the nature of the binding interaction between the pentasaccharide-binding region of antithrombin and heparin influences the efficiency of acylated strand 4A insertion and/or stable inhibitory complex formation. This possibility is consistent with previous studies showing that antithrombin exhibits increased substrate behavior in the presence of heparin (19, 32).

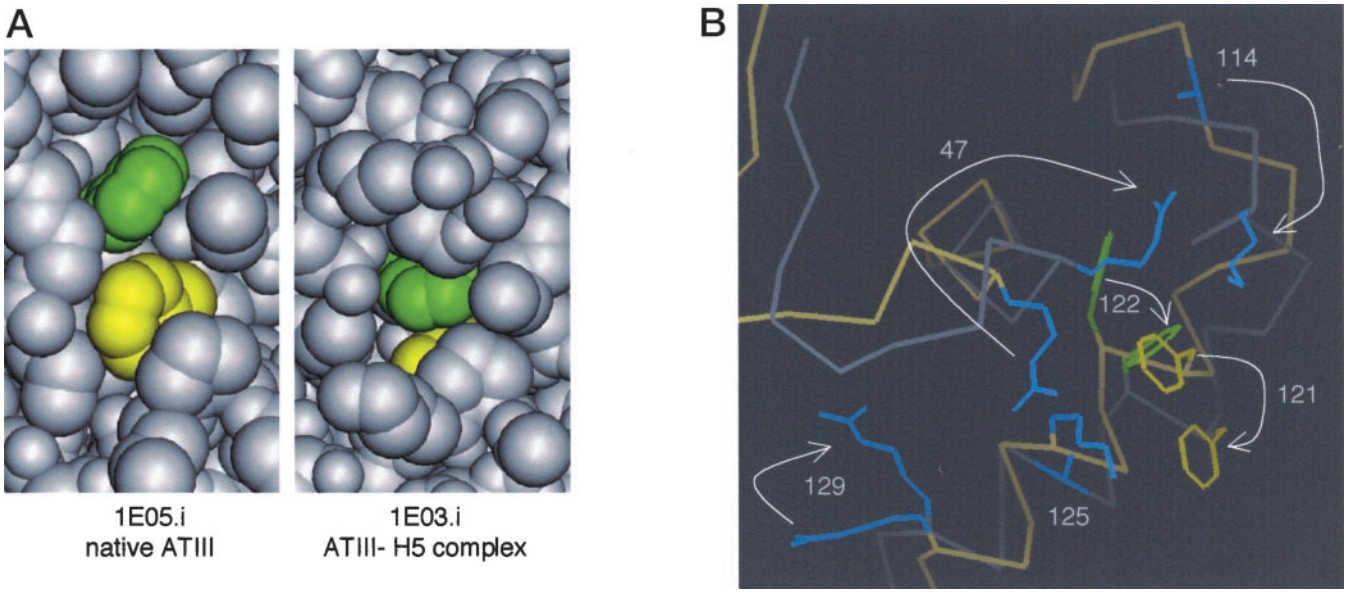

FIG. 4. *A*, Phe-121 and Phe-122 are partially exposed to solvent in the native conformation of antithrombin but shift to a more hydrophobic environment when heparin is bound. *Drawings* show the surface of antithrombin III in the Phe-121/Phe-122 region of the heparin binding site as viewed from the solvent. The *left panel* is the van der Waals surface for the *I*-chain of native human antithrombin III, not bound to heparin (pdb.1E05). The *right panel* shows the van der Waals surface from the structure of the *I*-chain of the human ATIII-pentasaccharide complex (pdb.1E03), with the overlying pentasaccharide removed to permit viewing. Phe-121 is *yellow*. Phe-122 is *green*. *B*, heparin binding and burial of Phe-121 and Phe-122 are accompanied by rearrangement of heparin binding site lysine and arginine residues. The structures of the *I*-chains of human antithrombin III unbound (pdb.1E05) and bound to pentasaccharide (pdb.1E03) were superpositioned using the entire sets of α carbon data and the least-squares algorithm in QUANTA software. The α carbon trace of native antithrombin III (not bound to pentasaccharide) is *yellow*. The α carbon trace of antithrombin III in complex with pentasaccharide is *gray*. Phe-121 is *yellow*, and Phe-122 is *green*. Arg-47, Lys-114, Lys-125, and Arg-129 are *blue*. The *arrows* illustrate the movement of individual residues from their positions in native antithrombin (*tails*) to their positions in the ATIII-pentasaccharide complex (*arrowheads*).

DISCUSSION

As illustrated in Fig. 3, phenylalanines 121 and 122 are located below the pentasaccharide and in the center of a cluster of positively charged residues (Arg-47, Lys-114, Lys-125, and Arg-129) known to participate in heparin binding (9–12, 33). To investigate the roles of Phe-121 and Phe-122 in heparin binding and activation of ATIII, we made F121A and F122L substitution mutants on a β-antithrombin-like N135A background. F121A/N135A and F122L/N135A association rates for inhibition of thrombin and factor Xa in the absence and presence of full-length heparin and pentasaccharide were similar to control, and SDS-stable inhibitory complexes with target enzymes formed, indicating proper folding and function with respect to proteinase inhibition. However, the mutants displayed distinct heparin binding and activation defects. F121A/N135A exhibited a 13-fold decrease and F122L/N135A exhibited a >2000-fold decrease in affinity for full-length heparin. In both cases, reduced binding was entirely due to the loss of non-ionic interactions (hydrogen bonds, van der Waals, and hydrophobic interactions), whereas the number of ionic interactions remained unchanged. For binding of full-length heparin to F122L/N135A under physiological conditions of pH and ionic strength, formation of the weak AT-H intermediate in the two-step-induced fit mechanism for heparin activation of ATIII occurs normally, as indicated by its normal K_1. However, a moderate reduction in the value of k_{+2} and a large increase in the value of k_{-2} revealed that the >2000-fold loss of binding affinity results from a ~20-fold reduction in the rate of the AT-H to AT*H conformational transition coupled with a >200-fold decrease in stability of the activated AT*H complex. The effects of the Phe-122 mutation on pentasaccharide binding are comparable to its effects on the binding of full-length heparin; however, in addition a slight decrease in the affinity of the first binding step is apparent for the pentasaccharide.

The findings of our work on the functional contributions of phenylalanines 121 and 122 to antithrombin heparin binding and activation were evaluated from a structural point-of-view using high resolution x-ray structures for human plasma α antithrombin bound (pdb.1E03) and not bound (pdb.1E05) to pentasaccharide. From this analysis, we have identified a series of Phe-121- and Phe-122-mediated non-ionic interactions that appear to make significant contributions to the strength of ATIII-heparin binding. The structural analysis also revealed several Phe-121- and Phe-122-helix P interactions that appear to be critical for the conformational activation step and stabilization of the high affinity AT*H complex, which were defective in the kinetic studies of the F122L/N135A mutant.

Phe-121 and Phe-122 Contributions to the Non-ionic Component of ATIII Heparin Binding—Fig. 3 shows that the most direct interaction between Phe-122 and the pentasaccharide involves the CZ of its phenylalanine side chain and the 3-*O*-sulfate on sugar F. Considering that extensive direct, non-ionic interactions between Phe-122 and the pentasaccharide are *not* observed in the co-crystal structure, it is paradoxical that the large loss of heparin binding affinity measured for the F122L mutant should be entirely accounted for by the loss of non-ionic interactions between ATIII and heparin (Table II). This disparity between the functional data and first inspection of the crystal structure can be resolved by hypothesizing that heparin makes non-ionic interactions with ATIII that do not directly involve the Phe-122 residue but are Phe-122-dependent.

Further examination of the co-crystal structure (Fig. 3) reveals that the distal carbons of the Phe-122 phenyl ring form van der Waals and hydrophobic interactions with the hydrocarbon stems of the Arg-47 and Lys-114 side chains, positioning their respective terminal guanidinium and amino groups for multiple ionic and hydrogen bond interactions with the pentasaccharide. Measurements of the packing of the Phe-122 phenyl ring against the alkyl side chains of Arg-47 and Lys-114 in the ATIII-pentasaccharide complex are presented in Table V. Table VI lists measurements for specific ionic and non-ionic interactions formed between the pentasaccharide and the Arg-47 guanidinium side chain or Lys-114 epsilon amino group as a result of their positioning by the hydrophobic interactions between Phe-122 and Arg-47 and between Phe-122 and Lys-114 described in Table V. The overall conclusion from the information in Fig. 3 and Tables V and VI is that non-ionic interactions between Phe-122 and the proximal stems of the Arg-47 and Lys-114 side chains lead to extensive and specific contacts of their distal charged groups and the pentasaccharide. In the case of Arg-47, the guanidinium position specified by the interaction of its stem and the Phe-122 phenyl ring leads to four ionic and two non-ionic interactions involving the F, G, and H sugars of the pentasaccharide (see Fig. 3 and the *right side* of Table VI). In the case of the Lys-114 side chain, three different ionic interactions and five different non-ionic interactions with the pentasaccharide form as the result of the epsilon amino position specified by interactions of Phe-122 with Lys-114 CD and CE. The ionic and non-ionic interactions of Lys-114

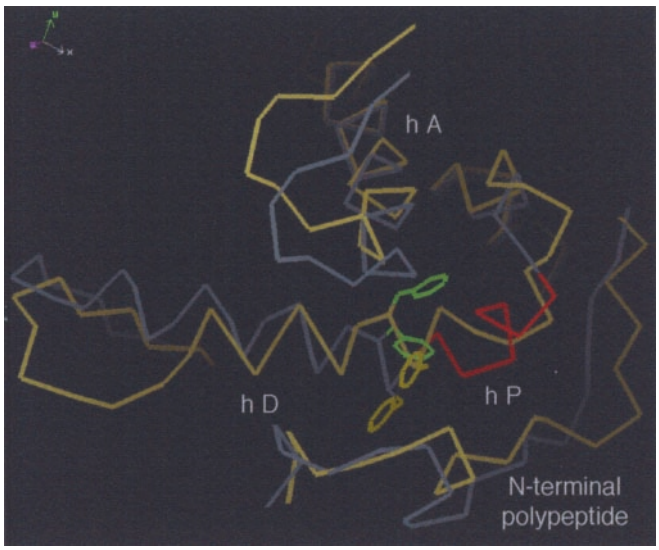

FIG. 5. **Phe-121 and Phe-122 are located in the center of the helix D, helix A, helix P, and N-terminal polypeptide structural elements that rearrange during the protein conformational change associated with heparin binding and activation.** The α carbon backbones of antithrombin III *I*-chains not bound (pdb.1E05) and bound to pentasaccharide (pdb.1E03) were superpositioned as above. Native, unbound ATIII backbone is *yellow*. The backbone of ATIII in complex with pentasaccharide is *gray*, except for residues 113–119, which form the P-helix and are drawn in *red*. Phe-121 is *yellow*, and Phe-122 is *green*. *hA* indicates helix A, *hD* indicates helix D, and *hP* indicates helix P.

TABLE VII
Phe-121 and Phe-122-P helix contacts

Distances between indicated atoms of Phe-121 and Phe-122 and P helix atoms were measured in the *I*-chain of the ATIII-pentasaccharide complex (pdb.1E03).

	P helix amino acid	Distance
		Å
F122_CD2	T115_CG2	3.6
F122_CE2	K114_CD	4.3
F122_CZ	K114_CE	4.7
F121_CB	Q118_CB	4.0

with the cofactor are distributed over the pentasaccharide F, G, and H sugars, as shown in Fig. 3 and on the *left side* of Table VI.

In the F122L variant the distal CZ, CE1, and CE2 carbons of the normally occurring phenylalanine side chain are missing. As shown in Table V, these are exactly the carbons that mediate van der Waals and hydrophobic bonding of Phe-122 with Lys-114 and Arg-47. In the absence of the intact Phe-122 phenyl ring, positioning of Arg-47 and Lys-114 to develop the full range of non-ionic interactions described in Table VI will occur less efficiently. Although the unchanged Z value of F122L/N135A indicates that the normal number of ionic interactions with the pentasaccharide form despite the substitution, the substantial K_d' increase suggests that the distal carbons of the phenylalanine ring are necessary for participating in affinity-augmenting hydrophobic/van der Waals interactions, and to precisely position the Lys-114 and Arg-47 epsilon amino and guanidinium groups for highly directional hydrogen bonding, which also contributes to the strength of the interaction. Thus, we propose that a substantial component of the >2000-fold loss in binding energy results from the reduced ability of the substituting leucine residue to specifically promote the ATIII-pentasaccharide van der Waals, hydrophobic, and hydrogen bond interactions listed in Table VI. With respect to Lys-114, affected interactions in the F122L/N135A mutant would include the hydrophobic interaction between the stem of the lysine and sugar H of the pentasaccharide, and a trifurcated hydrogen bond between its epsilon amino group and three sites on sugar G. For Arg-47, the bifurcated hydrogen bond between the Arg-47 guanidinium and two sulfates of the H sugar are disfavored in the F122L/N135A mutant.

Van der Waals and hydrophobic interactions between the hydrocarbon stem of lysine 125 and the phenyl rings of Phe-121 and Phe-122 may also organize its epsilon amino group for favorable ionic and non-ionic hydrogen bond interactions with the D, E, and F sugars of the pentasaccharide. However, it is not possible to address this issue directly by inspection of the pdb.1E03 co-crystal structure due to the absence of density for the Lys-125 side chain distal to its β carbon (see Fig. 3). The low electron density may be due to population of more than one conformation in pentasaccharide-bound ATIII. This appears possible based on the position of the Lys-125 Cα and Cβ atoms, and the potential of its epsilon amino group to form hydrogen bond or ionic interactions with multiple polar atoms on the D, E, and F sugars and different van der Waals/hydrophobic interactions with Phe-121 and Phe-122. The 13-fold loss of binding affinity observed for F121A relative to its N135A parent may result from the loss of hydrophobic and van der Waals interactions between the ring of Phe-121 and proximal carbons of the Lys-125 side chain and/or the failure of the epsilon amino group to be optimally positioned to hydrogen bond with the pentasaccharide.

*Proposed Roles of Phe-121, Phe-122, the P-helix and Lys-114 in the Heparin-dependent Conformational Change and Stabilization of AT*H*—*Fig. 4*A* shows that Phe-121 and Phe-122 are partially exposed to solvent in the native conformation of antithrombin (1E05.i, *left panel*) but shift to a more hydrophobic environment when heparin is bound (1E03.i, *right panel*). Burial of Phe-121 and Phe-122 is associated with movement of heparin binding site lysine and arginine residues (Fig. 4*B*) to positions in which extensive and specific ionic and non-ionic interactions with the pentasaccharide develop, as discussed above and enumerated in Table VI. Fig. 5 shows that Phe-121 and Phe-122 are located in the center of the helix D, helix A, helix P, and N-terminal polypeptide structural elements that rearrange during the protein conformational change associated with heparin binding and activation. In this central location, Phe-121 and Phe-122 are ideally situated to contribute to and to coordinate the conformational change leading to high affinity binding of heparin and increased reactivity of the reactive loop with target proteinases.

When heparin binds antithrombin III, a short, one-turn α helix is formed from residues 113–119 at the amino-terminal end of helix D (*red* Cα backbone in Figs. 3 and 5). This conformation-dependent helix is called the P-helix (13), and it is not present in native antithrombin (see Fig. 5) (34). Two naturally occurring mutants disrupt P-helix formation due to substitutions of serine 116 or glutamine 118 with the imino acid proline (35, 36). S116P and Q118P variant antithrombins exhibit heparin binding defects and cause thrombosis, suggesting that P-helix formation is important for heparin binding and for the physiological expression of antithrombin activity. Structural and kinetic considerations further suggest that P-helix formation is of central importance in the conformational change generating the high affinity activated AT*H complex and that Phe-122 and the key pentasaccharide binding residue lysine-114 act cooperatively in the formation of AT*H.

Fig. 4*B* and Table VII show that P-helix formation is accompanied by the development of close contacts between Phe-121/Phe-122 and P-helix residues, including Lys-114. In native ATIII, Phe-122 and Lys-114 are well separated (see *arrow tails* in Fig. 4*B*). However, in the complex with pentasaccharide, these residues have moved near to each other (see *arrowheads* in Fig. 4*B*), and the Phe-122 phenyl ring is in van der Waals/hydrophobic contact with the side chains of P-helix residues Lys-114 and Thr-115 (see Table VII). Similarly, Phe-121 and Gln-118 move into close contact with each other (4.0 Å, see Table VII) in the structure of the P-helix-containing pentasaccharide-bound complex. Thus, extensive contacts between Phe-122 and Lys-114 in the crystal structure of the ATIII-pentasaccharide complex, but not in the structure of native antithrombin, suggest that these residues act cooperatively to form the P-helix and to stabilize the activated AT*H complex. This hypothesis is supported by similar three order of magnitude increases in the values of k_{-2} (= k_{off}) for F122L/N135A (Table III) and K114A/N135A (11). Therefore, based on the structural and kinetic considerations reviewed above, we propose that Phe-122 and Lys-114 act cooperatively through non-ionic interactions to promote ATIII binding to the pentasaccharide via a P-helix-mediated protein conformational change mechanism that promotes the formation and stabilization of the activated, high affinity AT*H complex.

Conclusion—This work establishes the importance of hydrophobic residues Phe-121 and Phe-122 for heparin binding and shows that, under physiological conditions of pH and ionic strength, Phe-122 is critical for inducing a normal rate of conformational change and stabilizing the activated heparin-ATIII complex, AT*H. The rich network of contacts between Phe-122, Lys-114, and the pentasaccharide and P-helix may explain why high affinity binding to heparin and the protein conformational change leading to ATIII activation are intimately linked processes. In addition to aligning Lys-114 and Arg-47 to make the extensive ionic, hydrogen bond, and hydrophobic interactions with the pentasaccharide, Phe-122 and Lys-114 act cooperatively in the formation and stabilization of the P-helix, which promotes high affinity binding to heparin and may also be a key element in propagating the protein conformational change that increases reactive loop reactivity with target enzymes.

Acknowledgments—We thank Dr. James Herron for the use of his spectrofluorometer, Dr. Maurice Petitou for pentasaccharide, and Dr. James Huntington for introducing us to the 1E03 and 1E05 structures.

REFERENCES

1. Olson, S., and Shore, J. (1981) *J. Biol. Chem.* **256,** 11065–11072
2. Olson, S. T., Bjork, I., Sheffer, R., Craig, P. A., Shore, J. D., and Choay, J. (1992) *J. Biol. Chem.* **267,** 12528–12538
3. Koide, T., Odani, S., Takahashi, K., Ono, T., and Sakuragawa, N. (1984) *Proc. Natl. Acad. Sci. U. S. A.* **81,** 289–293
4. Peterson, C., Noyes, C., Pecon, J., Church, F., and Blackburn, M. (1987) *J. Biol. Chem.* **262,** 8061–8065
5. Gandrille, S., Aiach, M., Lane, D., Vidaud, D., Molho-Sabatier, P., Caso, R., Moerloose, P. D., Fiessinger, J., and Clauser, E. (1990) *J. Biol. Chem.* **265,** 18997–19001
6. Kridel, S., Chan, W., and Knauer, D. (1996) *J. Biol. Chem.* **271,** 20935–20941
7. Kridel, S., and Knauer, D. (1997) *J. Biol. Chem.* **272,** 7656–7660
8. Ersdal-Badju, E., Lu, A., Zuo, Y., Picard, V., and Bock, S. (1997) *J. Biol. Chem.* **272,** 19393–19400
9. Arocas, V., Bock, S., Olson, S., and Bjork, I. (1999) *Biochemistry* **38,** 10196–10204
10. Desai, U., Swanson, R., Bock, S., Bjork, I., and Olson, S. (2000) *J. Biol. Chem.* **275,** 18967–18984
11. Arocas, V., Bock, S., Raja, S., Olson, S., and Bjork, I. (2001) *J. Biol. Chem.* **276,** 43809–43817
12. Schedin-Weiss, S., Desai, U., Bock, S., Gettins, P., Olson, S., and Bjork, I. (2002) *Biochemistry* **41,** 4779–4788
13. Jin, L., Abrahams, J., Skinner, R., Petitou, M., Pike, R., and Carrell, R. (1997) *Proc. Natl. Acad. Sci., U. S. A.* **94,** 14683–14688
14. Belzar, K., Zhou, A., Carrell, R., Gettins, P., and Huntington, J. (2002) *J. Biol. Chem.* **277,** 8551–8558
15. vanBoeckel, C., Grootenhuis, P., and Visser, A. (1996) *Nat. Struct. Biol.* **1,** 423–425
16. Huntington, J., Olson, S., Fan, B., and Gettins, P. (1996) *Biochemistry* **35,** 8495–8503
17. Olson, S., and Bjork, I. (1991) *J. Biol. Chem.* **266,** 6353–6364
18. Hileman, R., Jennings, R., and Linhardt, R. (1998) *Biochemistry* **37,** 15231–15237
19. Turk, B., Brieditis, I., Bock, S., Olson, S., and Bjork, I. (1997) *Biochemistry* **36,** 6682–6691
20. Backovic, M., and Gettins, P. (2002) *J. Proteome Res.* **1,** 367–373
21. Jordan, R. (1983) *Arch. Biochem. Biophys.* **227,** 587–595
22. Jairajpuri, M., Lu, A., and Bock, S. (2002) *J. Biol. Chem.* **277,** 24460–24465
23. Ersdal-Badju, E., Lu, A., Peng, X., Picard, V., Zendehrouh, P., Turk, B., Björk, I., Olson, S., and Bock, S. (1995) *Biochem. J.* **310,** 323–330
24. Picard, V., and Bock, S. (1996) in *Methods in Molecular Biology: PCR Protocols* (White, B. A., ed) pp. 183–186, Humana Press, Totowa, NJ
25. Nordenman, B., Nystrom, C., and Bjork, I. (1977) *Eur. J. Biochem.* **18,** 195–203
26. Olson, S., Bjork, I., and Shore, J. (1993) *Methods Enzymol.* **222,** 525–560
27. Olson, S., Srinivasan, K., Bjork, I., and Shore, J. (1981) *J. Biol. Chem.* **256,** 11073–11079
28. Olson, S., and Shore, J. (1982) *J. Biol. Chem.* **257,** 14891–14895
29. Picard, V., Ersdal-Badju, E., and Bock, S. (1995) *Biochemistry* **34,** 8433–8440
30. Meagher, J. L., Beechem, J. M., Olson, S. T., and Gettins, P. G. W. (1998) *J. Biol. Chem.* **273,** 23283–23289
31. Arocas, V., Turk, B., Bock, S., Olson, S., and Bjork, I. (2000) *Biochemistry* **39,** 8512–8518
32. Olson, S. (1985) *J. Biol. Chem.* **260,** 10153–10160
33. Olson, S., Bjork, I., and Bock, S. (2002) *Trends Cardiovasc. Med.* **12,** 198–205
34. Skinner, R., Abrahams, J., Whisstock, J., Lesk, A., Carrell, R., and Wardell, M. (1997) *J. Mol. Biol.* **266,** 601–609
35. Okijama, K., Abe, H., Maeda, S., Motomura, M., Tsujihata, M., Nagataki, S., Okabe, H., and Takatsuki, K. (1993) *Blood* **81,** 1300–1305
36. Chowdhury, V., Mille, B., Olds, R., Lane, D., Watton, J., Barrowcliffe, T., Pabinger, I., Woodcock, B., and Thein, S. (1995) *Br. J. Haematol.* **89,** 602–609